# SCHEMES FOR CONVECTION DISCRETISATION IN PHOENICS

**M.R.Malin and N.P.Waterson***

*CHAM Limited, Bakery House, 40 High Street, Wimbledon, London SW19 5AU, UK*
** VKI, Chaussee de Waterloo, 72, 1640 Rhode-St-Genese, Belgium*

PHOENICS Version No: 2.2; Computer: PENTIUM PRO - 200MHz -32MB RAM

## ABSTRACT

This paper describes the convection-discretisation schemes provided by the authors for general use in PHOENICS V2.2 and later releases. This work, which was carried out in 1995, furnished PHOENICS with an extensive set of higher order schemes. In addition to the built-in upwind and hybrid differencing schemes, provision was made for five linear schemes and twelve non-linear schemes. These schemes are applicable to the convection of scalar and momentum variables on uniform and non-uniform, regular and BFC grids, with or without the presence of blocked or solid regions.

## 1. INTRODUCTION

An important consideration in CFD is the discretisation of the convection terms in the finite-volume equations. The accuracy, numerical stability and the boundedness of the solution depends on the numerical scheme used for these terms. The central issue is the specification of an appropriate relationship between the convected variable, stored at the cell centre, and its value at each of the cell faces.

The default scheme used in PHOENICS for all variables is the hybrid-differencing scheme (HDS), which employs the 1st-order upwind-differencing scheme (UDS) in high convection regions; and the 2nd-order central-differencing scheme (CDS) in low-convection regions. The UDS is bounded and highly stable, but highly diffusive when the flow direction is skewed relative to the grid lines. The HDS is only marginally more accurate than the UDS, as the 2nd-order CDS will be restricted to regions of low Peclet number.

The two approaches commonly used to remedy the problem of numerical diffusion are mesh refinement and the adoption of schemes with a higher order of accuracy than UDS. For engineering problems, the necessary degree of grid refinement to alleviate numerical diffusion is generally impractical as the UDS and HDS are rather sluggish to grid-refinement. Consequently, schemes with higher-order truncation errors than UDS have been proposed in an attempt to improve resolution.

Linear higher-order schemes, such as the CDS and the well-known QUICK scheme, increase the accuracy of the solution, but may suffer from the boundedness problem, i.e. the solution may display unphysical oscillations around steep gradients, or unacceptable negative values for species concentrations and certain turbulence quantities.

A number of approaches have been proposed to eliminate the boundedness problem. They can usually be classified as flux-blending methods (see Khosla & Rubin [1974]) or flux-limiter methods. The latter modify linear higher-order schemes by using a flux limiter, which enforces a boundedness criterion based on the local solution behaviour. The resulting scheme is therefore non-linear, and such schemes are usually formulated using either the flux-limiter diagram (see Sweby [1984]) or the normalised-variable diagram (see Leonard [1987] and Gaskell & Lau [1988]). The non-linear schemes in PHOENICS are based on the flux-limiter formulation of Roe [1987,1989]. This formulation differs from Sweby's [1984] in that the spatial terms are divorced from the time discretisation, as discussed by Waterson [1994].

In the past PHOENICS has been equipped with two different and restrictive options for higher-order convection schemes. In PHOENICS 2.2, these implementations were replaced by a unified approach which allows the implementation of a large variety of linear and non-linear schemes applicable to the convection of both scalar and momentum variables on uniform and non-uniform, regular and BFC grids, with or without the presence of blocked or solid regions.

These schemes may be used for both single- and two-phase flows, although the facility has yet to be extended to include the volume fraction equations R1, R2 and RS, and the energy variables TEM1 and TEM2. The other limitation is that there is no special treatment of the domain and internal boundaries, at which all higher-order schemes are reduced to the UDS.

Specifically, PHOENICS 2.2 and later releases provide for 5 alternative linear schemes, and 12 alternative non-linear schemes. The linear schemes are based on the Kappa formulation (see Van Leer [1985], Roe [1987]), and comprise CDS, QUICK, the cubic upwind scheme (CUS), the linear upwind scheme (LUS) and Fromm's [1968] scheme. The non-linear schemes extend the Kappa formulation so as to employ a flux limiter to secure boundedness (see Deconinck and Waterson [1995]) at the expense of reduced accuracy. The non-linear schemes currently available are: SMART, H-QUICK, UMIST, Koren, Superbee, Minmod, OSPRE, van Albada, MUSCL, CHARM, H-CUS and van-Leer harmonic.

This paper puts on record the work conducted to equip PHOENICS with an extensive set of higher-order schemes. In the remainder of this paper, Sections 2 to 6 provide a comprehensive mathematical description, Sections 7 and 8 deal with the implementation and activation of the numerical schemes, Sections 9 and 10 provide recommendations and exemplification, and finally, Section 11 provides concluding remarks.

## 2. FINITE-VOLUME EQUATIONS

For simplicity, the analysis is presented in terms of steady, single-phase flow. The conservation equation for a general specific variable $\phi$ can be written as:

$$\nabla.(\rho \mathbf{U}\phi - G\nabla\phi) = S \qquad (2.1)$$

where $\rho$ is the fluid density, **U** the fluid velocity vector, G is a diffusion exchange coefficient, and S the source term. This equation can be integrated over a control volume so as to produce the following discretised equation for $\phi$:

$$J_h - J_l + J_n - J_s + J_e - J_w + D_h - D_l + D_n - D_s + D_e - D_w = S_p \qquad (2.2)$$

where Sp is the source term for the control volume p, and $J_f$ and $D_f$ represent, respectively, the convective and diffusive fluxes of $\phi$ across the control-volume face f (f=h,l,n,s,e or w).

The convection fluxes through the cell faces are calculated as:

$$J_f = C_f \phi_f \qquad (2.3)$$

where $C_f$ is the mass flow rate across the cell face f. The convected variable $\phi_f$ associated with this mass flow rate is actually stored at the cell centres, and thus some form of interpolation assumption must be made in order to determine its value at each cell face. The interpolation procedure employed for this operation is the subject of the various schemes proposed in the literature, and the accuracy, stability and boundedness of the solution depends on the procedure used.

In general, the value of $\phi_f$ can be explicity formulated in terms of its neighbouring nodal values by a functional relationship of the form:

$$\phi_f = P(\phi_{nb}) \qquad (2.4)$$

where $\phi_{nb}$ denotes the neighbouring-node $\phi$ values.

Combining equations (2.2) through (2.4), the discretised equation becomes:

$$\{ D_h + C_h [P(\phi_{nb})]_h \} - \{ D_l + C_l [ P(\phi_{nb})]_l \} +$$

$$\{ D_n + C_n [P(\phi_{nb})]_n \} - \{ D_s + C_s [P(\phi_{nb})]_s \} +$$

$$\{ D_e + C_e [P(\phi_{nb}) ]_e \} - \{ D_w + C_w [P(\phi_{nb})]_w \} = S_p \qquad (2.5)$$

In PHOENICS, the higher-order schemes are introduced into equation (2.5) by using the deferred-correction procedure of Rubin and Khosla [1982]. This procedure expresses the cell-face value $\phi_f$ by:

$$\phi_f = \phi_f(U) + \phi_f' \qquad (2.6)$$

where $\phi_f'$ is a higher-order correction which represents the difference between the UDS face value $\phi_f(U)$ and the higher-order scheme value $\phi_f(H)$, i.e.

$$\phi_f' = \phi_f(H) - \phi_f(U) \qquad (2.7)$$

If equation (2.6) is substituted into equation (2.5), the resulting discretised equation is:

$$\{ D_h + C_h \phi_h(U) \} - \{ D_l + C_l \phi_l(U) \} + \{ D_n + C_n \phi_n(U) \} - \{ D_s + C_s \phi_s(U) \}$$

$$+ \{ D_e + C_e \phi_e(U) \} - \{ D_w + C_w \phi_w(U) \} = S_p + B_p \qquad (2.8)$$

where $B_p$ is the deferred-correction source term, given by:

$$B_p = C_l\phi_l' - C_h\phi_h' + C_s\phi_s' - C_n\phi_n' + C_w\phi_w' - C_e\phi_e' \qquad (2.9)$$

This treatment leads to a diagonally dominant coefficient matrix since it is formed using the UDS.

If equation (2.8) is expanded in terms of nodal values, the final form of the discretised equation is:

$$a_p\phi_p = \sum(a_{nb}\phi_{nb}) + S_p + B_p \qquad (2.10)$$

where: $a_p$ and $a_{nb}$ are the convection-diffusion coefficients obtained from the UDS: $\phi_p$ is the cell-average value of $\phi$ stored at the cell centre; and the summation is over the immediate neighbouring nodes nb (=L,H,S,N,W and E).

All of the schemes provided in PHOENICS calculate the cell-face values $\phi_f$ using at most three cell-centre values, namely: the upstream, central and downstream grid points, designated by u, c and d respectively. The cell-face location f lies between the central and downstream grid points.

## 3. CENTRAL-, UPWIND- AND HYBRID-DIFFERENCING SCHEMES

*Central Differencing Scheme:* The most natural assumption for the cell-face value of the convected variable $\phi_f$ would appear to be the CDS, which calculates the cell-face value from:

$$\phi_f = 0.5 (\phi_c + \phi_d) \qquad (3.1)$$

This scheme is 2nd-order accurate, but is unbounded so that unphysical oscillations appear in regions of strong convection and also in the presence of discontinuities, such as shocks. The CDS may be used directly in very low Reynolds-number flows where diffusive effects dominate over convection.

*Upwind Differencing Scheme*: The UDS (see Courant et al [1952]) assumes that the convected variable at the cell face f is the same as the upwind cell-centre value:

$$\phi_f = \phi_c \qquad (3.2)$$

The UDS is unconditionally bounded and highly stable, but as noted earlier it is only 1st-order accurate in terms of truncation error and may produce severe numerical diffusion. The scheme is therefore highly diffusive when the flow direction is skewed relative to the grid lines.

*Hybrid Differencing Scheme*: The HDS of Spalding [1972] switches the discretisation of the convection terms between CDS and UDS according to the local cell Peclet number, as follows:

$$\begin{aligned} \phi_f &= 0.5\,(\phi_c + \phi_d) \quad \text{for} \quad Pe < 2 \\ \phi_f &= \phi_c \quad \text{for} \quad Pe > 2 \end{aligned} \tag{3.3}$$

The cell Peclet number is defined as:

$$Pe = \rho\, abs(U_f)\, A_f/D_f \tag{3.4}$$

in which $A_f$ and $D_f$ are, respectively, the cell-face area and physical diffusion coefficient. When Pe > 2, CDS calculations tend to become unstable so that the HDS reverts to the UDS. Physical diffusion is ignored when Pe > 2.

The HDS scheme is marginally more accurate than the UDS, because the 2nd-order CDS will be used in regions of low Peclet number.

## 4. CLASSIFICATION OF HIGHER-ORDER SCHEMES

Higher schemes can be classified as *linear* or *non-linear*, where *linear* means their coefficients are not direct functions of the convected variable when applied to a linear convection equation. It is important to recognise that linear convection schemes of 2nd-order accuracy or higher may suffer from unboundedness, and are not unconditionally stable.

*Non-linear* schemes analyse the solution within the stencil and adapt the discretisation to avoid any unwanted behaviour, such as unboundedness (see Waterson [1994]). These two types of scheme may be presented in a unified way by use of the *Flux-Limiter* formulation (Waterson and Deconinck [1995]), which calculates the cell-face value of the convected variable from:

$$\phi_f = \phi_c + 0.5B(r)\,(\phi_c - \phi_u) \tag{4.1}$$

where B(r) is termed a limiter function, and the gradient ratio r is defined as:

$$r = (\phi_d - \phi_c)/(\phi_c - \phi_u) \tag{4.2}$$

The generalisation of this approach to handle non-uniform meshes has been given by Waterson [1994].

From equation (4.1) it can be seen that B=0 gives the UDS and B=r gives the CDS.

## 5. LINEAR HIGHER-ORDER SCHEMES

PHOENICS provides the following linear higher-order schemes:

- CDS;
- Linear Upwind Scheme (LUS);
- Quadratic Upwind Scheme (QUICK);
- Fromm's Upwind Scheme; and
- Cubic Upwind Scheme.

All of the foregoing schemes are unified for implementation purposes as members of the Kappa class of schemes:

$$B(r) = 0.5 \{ (1 + K)r+(1 - K) \} \quad (5.1)$$

with K = 1 for *CDS*, K = 1/2 for *QUICK*; K = -1 for *LUS*, K = 0 for *Fromm*; and K = 1/3 for *CUS*. Consequently, B(r)=0 gives UDS, B(r)=1 gives LUS, and B(r)=r gives the CDS.

The linear schemes appear as straight lines in the Flux-Limiter Diagram (FLD) which takes the form of a plot of B(r) against r (see for example Hirsch [1990]). The two main regions of this diagram are given by r<0, indicating an extremum, and r>0 indicating monotonic variation. The linear schemes provided in PHOENICS are plotted in the Flux-Limiter Diagram of Figure 5.1.

*Kappa Schemes:* The Kappa formulation calculates the cell-face value $\phi_f$ as the sum of the upwind value and a higher-order correction:

$$\phi_f = \phi_c + \{0.25 (1+K) (\phi_d - \phi_c) + 0.25 (1-K) (\phi_c - \phi_u)\} \quad (5.2)$$

where K is a real number in the range: -1 <= K <= 1.

The Kappa class of schemes has as its extremes CDS (K=1), with no upwind bias, and LUS (K=-1), with complete upwind bias. Other members of the class may be viewed as weighted averages of these two schemes. All of these schemes require a 5-point stencil in one dimension (with the exception of K=1, which requires only 3), and all schemes are 2nd-order accurate, with the exception of K=1/3 (Agarwal[1981]), which is 3rd-order.

*Linear Upwind Scheme:* The LUS (see Price et al [1966]) calculates the face value of the convected variable by linear extrapolation from the two upwind cell-centre values:

$$\phi_f = \phi_c + 0.5(\phi_c-\phi_u) \quad (5.3)$$

and is therefore completely upwind biased, with no account taken of downstream influences. The scheme is often referred to as the 2nd-order upwind scheme.

*Quadratic Upwind Scheme:* The QUICK (Quadratic Upwind Interpolation for Convection Kinematics) scheme of Leonard [1978,1979] uses a quadratic fit through two upwind nodes and one downwind cell centre:

$$\phi_f = \phi_c + (3\phi_d - 2\phi_c - \phi_u)/8 \quad (5.4)$$

This scheme is 2nd-order accurate if the definition of truncation error is based on approximating the spatial derivative at cell centres in the linear convection equation (see Waterson [1994]). Other authors (see Leonard [1979], Gaskell & Lau[1988]) have chosen alternative definitions of the truncation error, according to which QUICK becomes 3rd-order accurate.

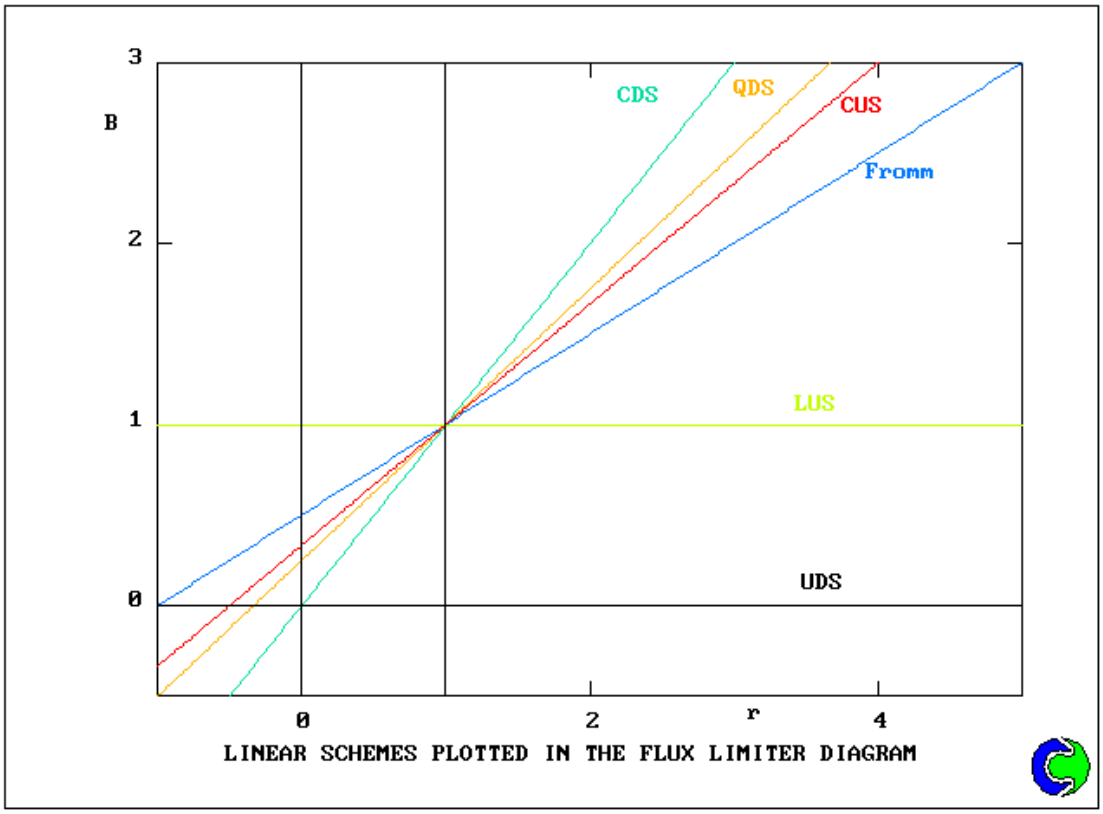


**Figure 5.1: Linear Schemes plotted in the Flux Limiter Diagram**

## 6. NON-LINEAR SCHEMES

Table 6.1 lists the non-linear schemes which have been provided in PHOENICS, while Figures 6.1 to 6.3 present the various schemes in the Flux-Limiter Diagram.

| Scheme | B(r) | Notes |
|---|---|---|
| SMART | max(0,min(2r, 0.75r+0.25, 4)) | Gaskell & Lau [1988]): bounded QUICK, piecewise linear |
| H-QUICK | 2 (r+\|r\|)/(r+3) | Waterson & Deconinck [1995]; harmonic based on QUICK, smooth |
| UMIST | max( 0, min(2r, 0.25+0.75r, 0.75+0.25r, 2) ) | Lien & Leschziner [1994]; bounded QUICK, piecewise linear |
| CHARM | $r(3r+1)/(r+1)^2$ for r > 0;<br>B(r) = 0. for r <= 0 | Zhou [1995]; bounded QUICK, smooth |
| MUSCL | max( 0, min( 2r, 0.5+0.5r, 2) ) | van Leer [1979]; bounded Fromm |
| Van-Leer harmonic | (r+\|r\|)/(r+1) | bounded Fromm |
| OSPRE | $3 (r^2+r)/\{2.(r^2+r+1)\}$ | Waterson & Deconinck [1995]; bounded Fromm |
| van Albada [1982] | $(r^2+r)/(r^2+1)$ | van Albada [1982]; bounded Fromm |
| Superbee | max( 0, min(2r,1), min(r,2) ) | Roe [1986], Hirsch [1990] |
| Minmod | max( 0, min(r, 1) ) | Roe [1986], Hirsch [1990] |
| H-CUS | 1.5 (r+\|r\|)/(r+2) | Waterson & Deconinck [1995]; bounded CUS |
| Koren | max( 0, min( 2r, 2r/3+1/3, 2) ) | Koren [1993]; bounded CUS |

**Table 6.1: PHOENICS Non-Linear Schemes**

The van-Leer harmonic, Minmod and MUSCL schemes are in fact identical to the later Normalised-Variable-Diagram schemes, respectively: HLPA (Zhu [1992]), SOUCUP (Zhu and Rodi [1991]) and MLU (Noll [1992]).

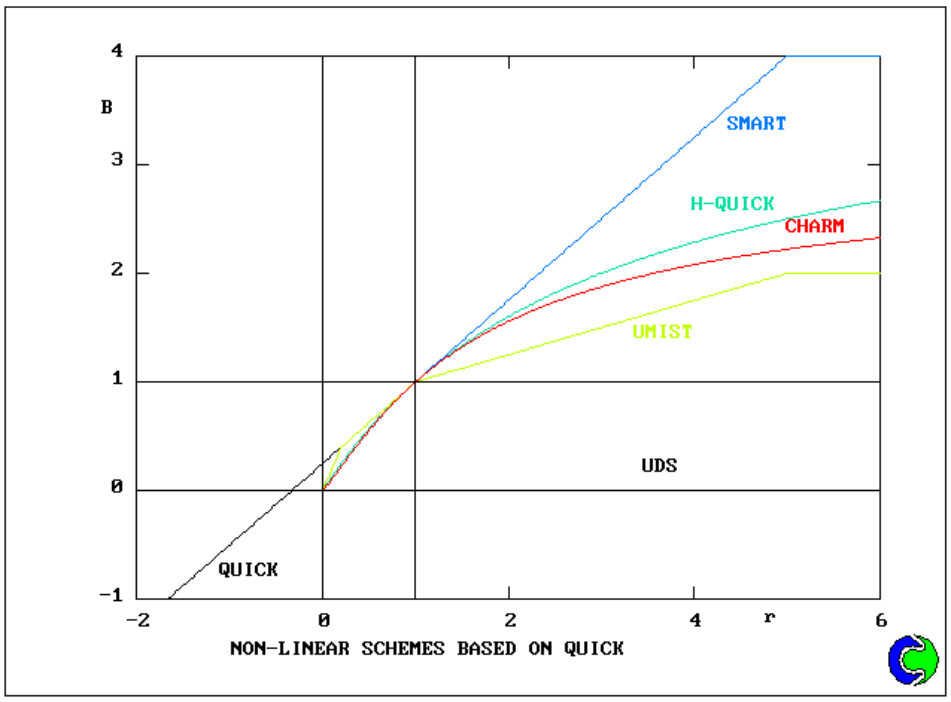


**Figure 6.1: Non-Linear Schemes based on QUICK in the Flux-Limiter Diagram**

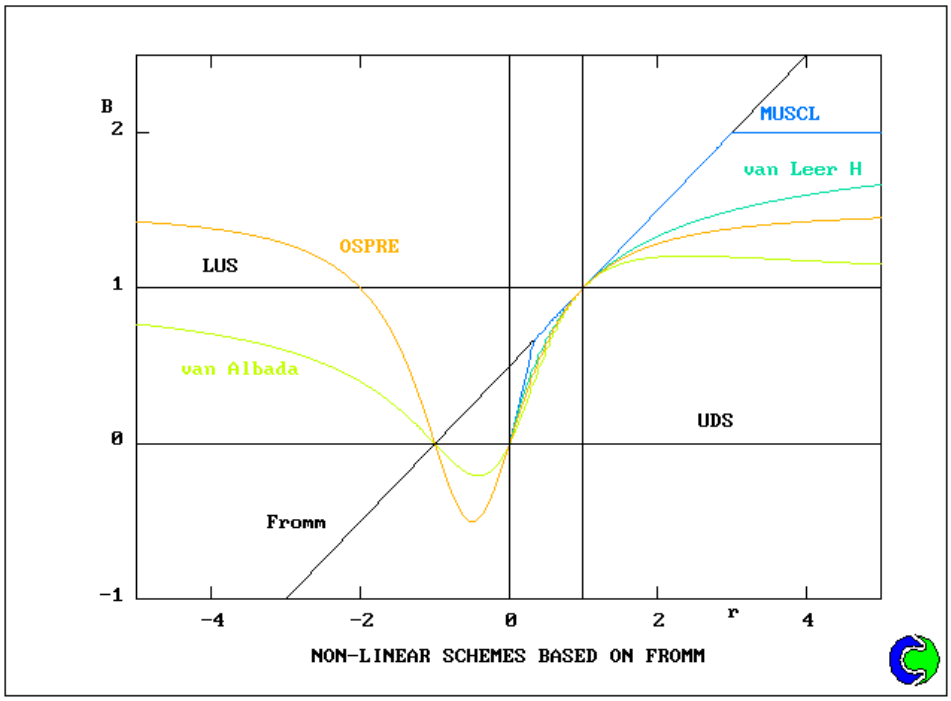


**Figure 6.2: Non-Linear Schemes based on Fromm in the Flux-Limiter Diagram**

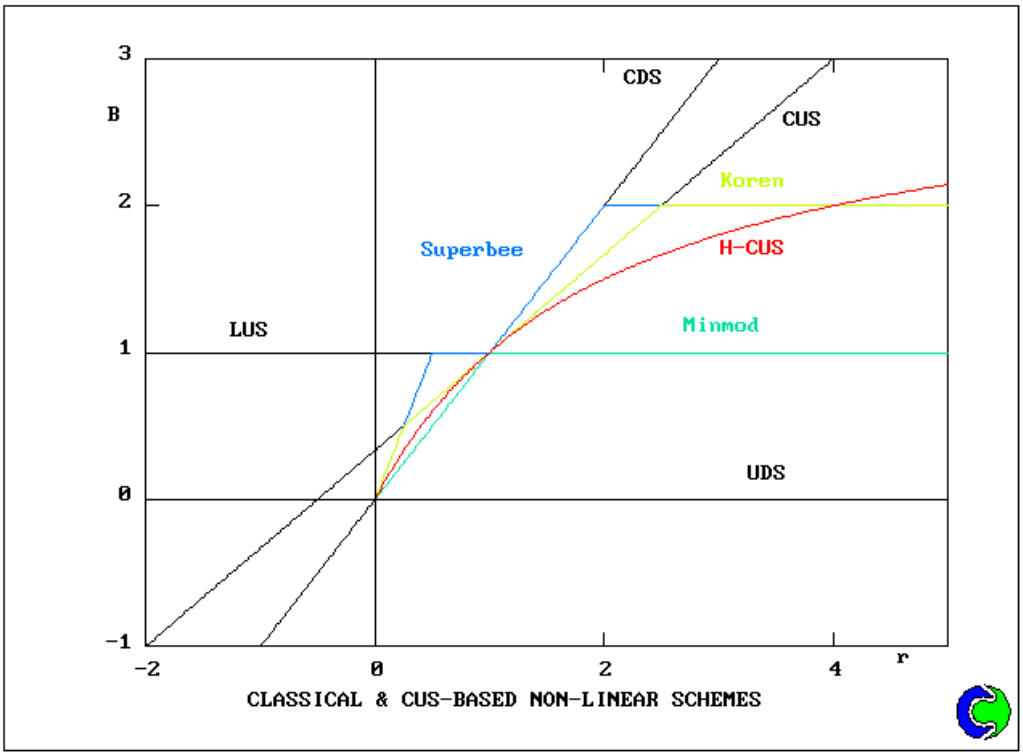


**Figure 6.3: Miscellaneous Non-Linear Schemes plotted in the Flux Limiter Diagram**

Waterson & Deconinck [1995] argue that most limiters fall into the following two categories:

- Polynomial ratio (PR) limiters, which offer the possibility of smooth, continuous limiter functions without discontinuous switching, thereby aiding convergence; and

- Piecewise-linear (PL) limiters which switch between linear schemes so as to produce bounded versions of existing linear schemes. The disadvantage is that their discontinuous nature may induce convergence problems.

The van Leer harmonic and OSPRE limiters are symmetric PR limiters, by which is meant that the forward and backward gradients are treated in the same manner, i.e. $B(r) = r\,B(1/r)$.

The H-QUICK and H-CUS limiters are non-symmetric harmonic limiters which are designed to be tangential at r=1 to QUICK and CUS respectively.

The UMIST and MUSCL limiters are symmetric PL limiters, whereas the SMART and Koren limiters are non-symmetric PL limiters.

The Minmod scheme is a composite of the UDS, CDS and LUS, and these three schemes are also involved in the Superbee scheme.

The CHARM scheme may be classed as a non-symmetric PR limiter which is tangential to QUICK at r=1, and reverts to the UDS for r < 0. This has been used with some success by Zhou [1995] for shock-capturing problems.

Limiter functions are designed to fulfil particular boundedness criteria, usually either the Total-Variation Diminishing (TVD) (Harten[1984], Sweby[1984]) or Positivity (Spekreijse [1986]) conditions.

These conditions prescribe regions on the FLD bounded by straight lines (see Hirsch [1990]). Deconinck and Waterson [1995] suggest that the TVD criterion is unnecessarily restrictive, as Sweby's TVD region in the FLD is entirely contained by the Positivity region.

All flux-limited schemes provided in PHOENICS are positive, and the following schemes are TVD: Koren, MUSCL, van Leer harmonic, Minmod, Superbee and UMIST.

The Superbee scheme forms the upper limit of the TVD diagram, and is known to have excellent resolution properties for discontinuities.

## 7. IMPLEMENTATION OF THE SCHEMES

The implementation strategy adopted in PHOENICS is to set DIFCUT=0 so as to retain the UDS for use in the built-in convection terms, and then to introduce the required higher-order modifications to this scheme in the form of an additional deferred-correction source term.

For details concerning the treatment of non-uniform meshes and BFCs, the reader is referred to Waterson [1994].

The higher-order convection schemes are coded in the GX-file GXHOCS.FOR, which comprises subroutine GXHOCS and its ancillary routines GXHOEN, GXHOHL, GXFLPS and BLKSLD.

Subroutine GXHOCS is called from Group 1 Section 1 and Group 13 Sections 13 and 14 of Subroutine GREX3.

In Group 1 Section 1, GXHOCS forms the array INLCS(NPHI) and allocates storage for several geometrical quantities. The array INLCS contains an integer, which defines for each variable the scheme selected by the user from the Menu or in Q1 via the SCHEME PIL command.

In Group 13, the deferred-correction source terms are calculated in Section 13 for linear schemes, and in Section 14 for non-linear schemes. Subroutine GXHOEN computes the east/west and north/south cell-face contributions to the source term, and Subroutine GXHOHL computes the low and high cell-face contributions.

Subroutine GXFLPS is called directly from Subroutines GXHOEN and GXHOHL so as to calculate the flux-limiter function for the non-linear schemes.

Function BLKSLD is used by subroutines GXHOEN and GXHOHL so as to detect the presence of blocked faces and solid cells within the stencil used to calculate the higher-order correction for a single-cell face. If BLKSLD is .TRUE., then no higher-order correction is calculated and the scheme reduces to the UDS.

## 8. SCHEME ACTIVATION

The PIL command SCHEME is used to select the required higher-order scheme for a SOLVEd-for variable. The user may also select higher-order schemes from the PHOENICS MENU. The default scheme for all variables is the HDS, which is activated by the setting DIFCUT=0.5. The UDS is activated for all variables by setting DIFCUT=0. The MENU provides a default setting of higher-order schemes, namely: VANLH for all variables.

A particular higher-order scheme is assigned to one or more dependent variables by the SCHEME command, whose syntax is:

SCHEME(NAME,variable name 1,variable name 2,...etc.)

The 1st argument NAME identifies the required discretisation scheme, as follows:

*Linear schemes*

NAME = LUS, FROMM, CUS, QUICK or CDS

*Non-linear schemes*

NAME = SMART, HQUICK, UMIST, KOREN, SUPBEE, MINMOD, OSPRE, VANALB, VANL1 (or MUSCL), VANL2 (or VANLH), CHARM, or HCUS.

The 2nd argument permits the user to specify those SOLVEd variables , which will use the selected scheme. If ALL is entered as the 2nd argument, then the selected scheme is applied to all SOLVEd-for variables. For example,

SCHEME(QUICK,U1,V1);SCHEME(SMART,H1,C1,C2)

selects QUICK for U1 and V1, and SMART for H1,C1 and C2, and UDS for any SOLVEd variables, which do not appear in a SCHEME command.

The SCHEME command is equivalent to:

DIFCUT=0.;PATCH(HOCS,CELL,1,NX,1,NY,1,NZ,1,LSTEP)

with COVAL(HOCS,PHI,FIXFLU,GRND1) for linear schemes; and COVAL(HOCS,PHI,FIXFLU,GRND2) for non-linear schemes.

The SCHEME command also assigns an appropriate scheme number, ISCHEM, to each variable as follows:

| Scheme | Type | ISCHEM |
|---|---|---|
| LUS | Linear | 1 |
| FROMM | " | 2 |
| CUS | " | 3 |
| QUICK | " | 4 |
| CDS | " | 5 |
| SMART | Non-Linear | 6 |
| KOREN | " | 7 |
| VANL1/MUSCL | " | 8 |
| HQUICK | " | 9 |
| OSPRE | " | 10 |
| VANL2/VANLH | " | 11 |
| VAN ALBADA | " | 12 |
| MINMOD | " | 13 |
| SUPBEE | " | 14 |
| UMIST | " | 15 |
| HCUS | " | 16 |
| CHARM | " | 17 |

The array INLCS(NPHI) is used to store the scheme number, and this information is then transmitted from SATELLITE to the GREX file GXHOCS by way of the SPEDAT facility. i.e.

```
SPEDAT(SET,SCHEME,INLCS//IVAR,I,ISCHEM)
```

where IVAR is a character variable of length 2, which is equal to the number of the SOLVEd-for variable. Thus, for example, INLCS03 corresponds to the variable U1 and INLCS07 to the variable W1.

If BFC=T then SCHEME arranges unconditional storage of: the Cartesian velocity components UCRT, VCRT and WCRT; and the grid-aligned velocity components UCMP, VCMP and WCMP. These components are required in the FORTRAN coding supplied in subroutine GXHOCS.

## 9. RECOMMENDATIONS

The selection of a suitable higher-order scheme involves a compromise between accuracy and numerical stability. The scheme should be accurate enough to provide significantly better resolution than the UDS, but without producing spurious oscillations in the solution and/or severe convergence problems.

The linear higher-order schemes offer good resolution, but are unbounded and likely to produce unphysical oscillations in regions of steep gradients, which can lead to

severe convergence problems. Therefore, it is recommended that non-linear (bounded) schemes always be applied to:

- the momentum equations whenever physical discontinuities are present, as for example in shock waves;

- those turbulence transport equations for which negative values are unacceptable, e.g. k, ε and the Reynolds normal stresses; and

- the species concentrations and enthalpy equations for which bounded solutions are essential.

For incompressible flows it is recommended that a linear higher-order scheme is applied to the momentum equations, unless severe convergence difficulties are encountered, in which case the user should employ a non-linear (bounded) scheme.

Of the linear higher-order schemes, the CUS is formally the most accurate according to truncation error, although QUICK gives similar results. The LUS is somewhat less accurate than these schemes, but gives much better numerical stability.

Of the non-linear schemes, the piecewise-linear, kappa-based schemes, SMART, Koren and MUSCL are likely to give the highest levels of accuracy. However, the smooth limiters, such as OSPRE and van Leer Harmonic, are likely to give much better convergence behaviour at somewhat reduced accuracy.

Minmod and Superbee not recommended for general use: Minmod because it is diffusive and slow to converge, and Superbee because it is over-compressive and will therefore sharpen physically-smooth gradients. Superbee is however excellent for sharp-interface problems e.g. free-surface scalar markers.

It should always be possible to obtain convergence when using the higher-order schemes from the very start of the calculation. Typically, the false time-step requirements are between 0.01 and 0.1 of the value required by the UDS or HDS. If convergence proves particularly problematic, then it is suggested that the user try restarting the calculation from a UDS or HDS solution.

## 10. EXEMPLIFICATION

The 'Numerical-Algorithms' library contains the Q1 files shown in Table 10.1 which exemplify the use of the higher-order schemes.

Any of these cases may be loaded from the LIBRARY MENU, or alternatively from the SATELLITE in interactive mode by typing, for example, LOAD(N110).

The results of library cases N101 to N104 inclusive may be found in the PHOENICS Applications Album by clicking on ‘Applications’ and then on ‘Numerical Methods’.

| Library Case Title | Number |
|---|---|
| 2d Diagonal Scalar Convection | N101 |
| 2d Laminar Wall-Driven Cavity | N102 |
| 2d Laminar Backward Facing Step | N103 |
| 2d Scalar Convection with Recirculation | N104 |
| 2d Turbulent Backward Facing Step | N105 |
| 2d Laminar Wall-Driven Cavity ( consistency tests ) | N106 |
| 2d Turbulent Backward Facing Step ( consistency tests ) | N107 |
| 2d Laminar Flow Over a Thin Fence ( consistency tests ) | N108 |
| 2d Laminar Wall-Driven Cavity ( BFC consistency tests ) | N109 |
| 2d Turbulent Flow through an Orifice Plate | N110 |
| 1d Shock-free transonic flow in a Laval nozzle | N111 |
| 1d Shocked transonic flow in a Laval nozzle | N112 |
| 2d Transonic underexpanded free jet | N113 |
| 2d Bluff-body stabilised methane jet | N114 |
| 2d Diagonal Scalar Convection (BFC test) | N115 |
| 2d Uniform Flow through a Box (BFC test) | N116 |
| 2d Uniform Flow across a Skewed Box (BFC test) | N117 |

**Table 10.1: PHOENICS Library of Q1 Input files**

**N101: 2D Diagonal Scalar Convection:** The problem concerns the 2d pure convection of a step profile of a scalar by a unidirectional and uniform flow field, which forms an angle 45 degrees with the horizontal axis. Since physical diffusion is absent, no mixing layer should form and the scalar discontinuity should persist in the streamwise direction. The Q1 example compares the solution for 6 different linear schemes and 9 non-linear schemes. The predicted concentration contours are compared in Figure 10.1 for the UDS and the Superbee scheme. It is evident that the UDS suffers from significant numerical diffusion.

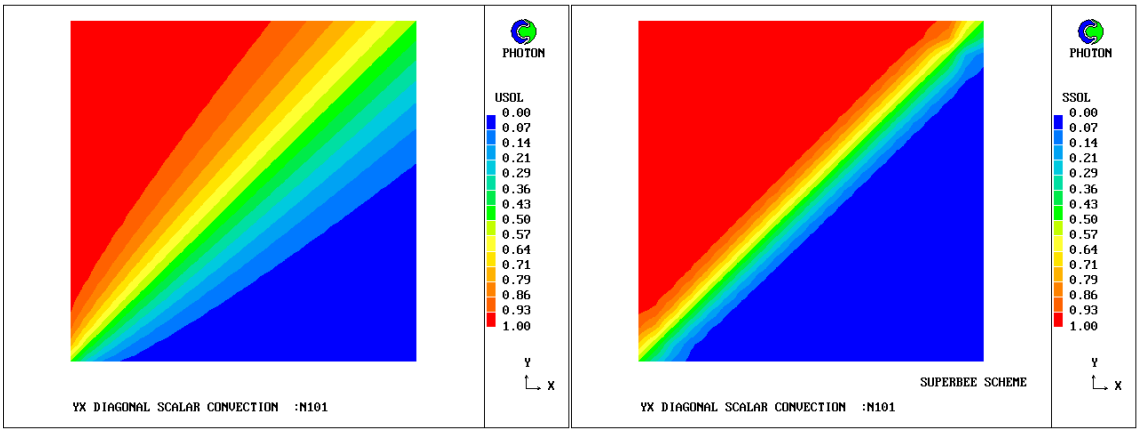


**Figure 10.1: Diagonal Scalar Convection: Concentration Contours for the UDS and Superbee Scheme.**

Figure 10.2 compares predicted concentration profiles at x/L=0.5 for selected schemes with the exact solution. The figures reveals that the CDS and Superbee schemes show closest agreement with the exact solution, although the CDS produces non-physical under- and overshoots.

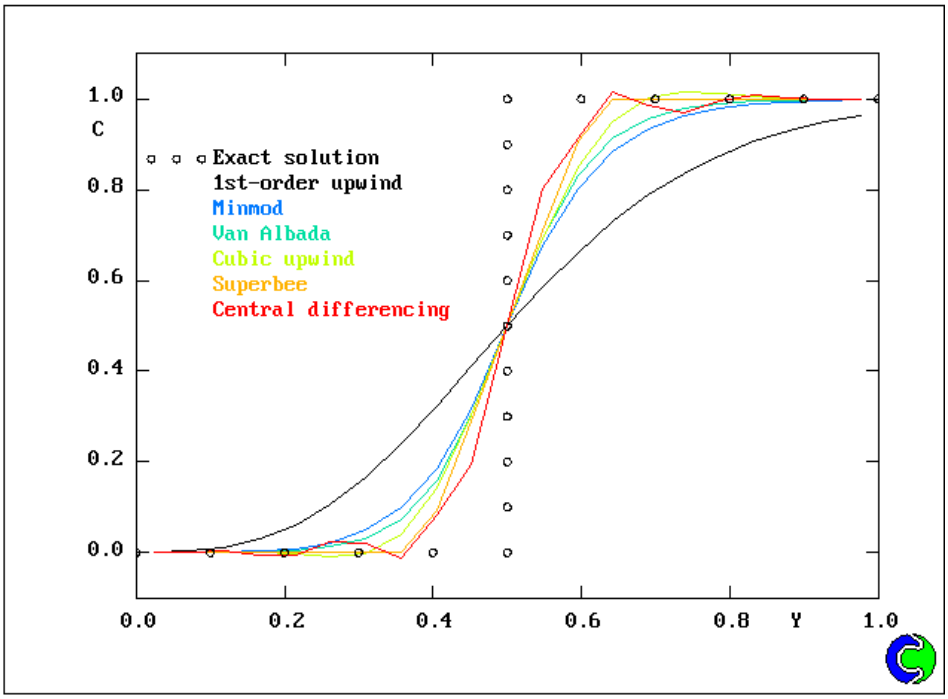


**Figure 10.2: Diagonal Scalar Convection: Concentration Profiles at X/L=0.5.**

**N102: 2D Laminar Wall-Driven Cavity:** This case considers 2d steady, incompressible, laminar recirculating flow inside a lid-driven cavity. The geometry is a 1m square cavity with no inflow or outflow. The flow is driven by a moving wall of -1m/s at the top of cavity. The Reynolds number based on cavity height is 1000. Calculations are performed with 3 linear schemes (CUS, UDS or QUICK) or 2 non-linear schemes (Koren or MUSCL). This case is a widely-used test problem for assessing the accuracy and stability of various numerical methods. It serves as a useful test case owing to the substantial skewness of the flow streamlines relative to the Cartesian mesh. The numerical results of Ghia et al (1982) for Re=100, 400, 1000, 3200 and 5000 are used by researchers as benchmark solutions.

For Re=1000, Figure 10.3 compares the horizontal velocity profiles at mid-cavity width with the exact of solution of Ghia et al (1982) on a relatively coarse mesh of 21 by 21 cells. The results show that the CUS gives the best and reasonably close agreement with the numerical data. The UDS produces a very diffusive solution, and consequently severely underestimates the peak value of the horizontal velocity.

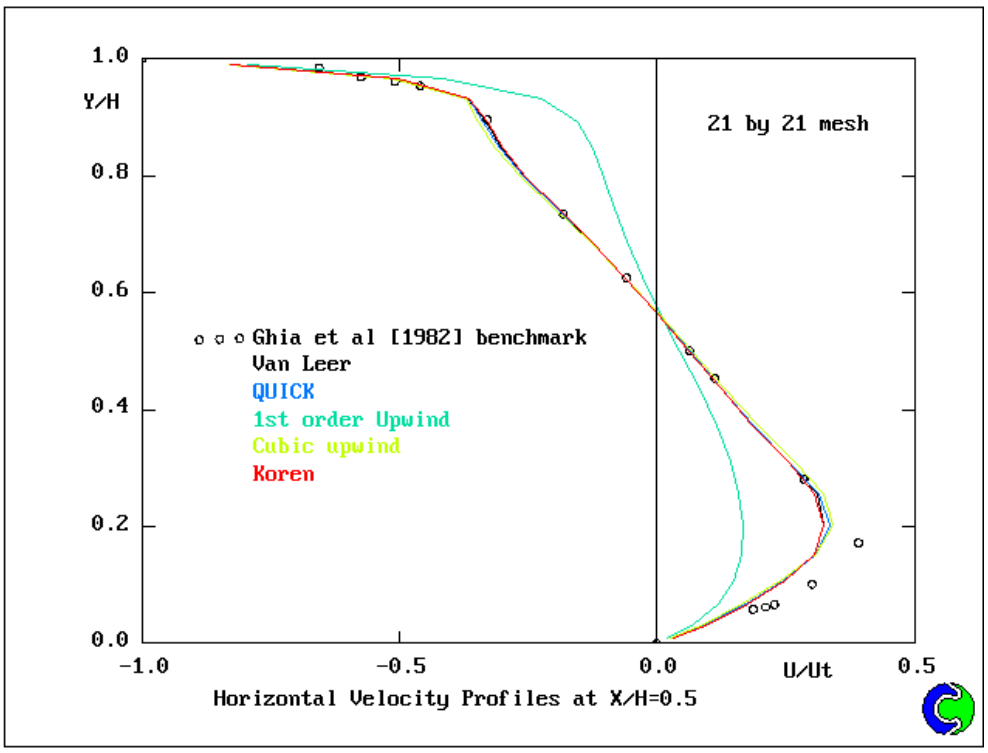


**Figure 10.3: Laminar Wall-Driven Cavity: Horizontal Velocity Profiles at Mid-Cavity Width**

**N103: 2D Laminar Backward-Facing Step:** The case considered is 2d steady incompressible, laminar backward-facing-step flow, i.e. flow through a straight channel having a sudden asymmetric expansion. The flow is characterised by the step height H and the Reynolds number Re, which is based on the bulk inlet velocity and 2h, where h is the flow inlet height. The channel expansion ratio is 1.94, and the total length of the domain is 40H. A fully-developed parabolic velocity profile is prescribed at the inlet boundary located at the step.

This test problem is widely used for assessing the accuracy of numerical methods because of the dependence of the reattachment lengths X on Re. The flow has been studied experimentally by Armaly et al (1983), and numerically in several papers (see for example, Gartling (1990), Freitas (1995) and Gresho et al (1993)).

Calculations are made on a mesh of 32 by 200 cells for comparison with Armaly's data at Re=150 and Re=450 using the HDS, CUS and the Van Albada scheme. At Re=150, a primary recirculation zone develops immediately downstream of the step with $X_1/H=5.0$. At Re=450, $X_1/H=9.5$ and an additional separation cell forms on the upper wall of the channel. The measurements indicate that the separation point of this cell is located at $X_2/H=7.6$ and the reattachment point at $X_3/H=11.3$, yielding a cell length of $dX/H=3.7$. The main results of the calculations are summarised below and compared with the measurements:

| Re=150 | Data | Hybrid | Cubic Upwind | Van Albada |
|---|---|---|---|---|
| $X_1/H$ | 4.2 | 4.17 | 4.24 | 4.25 |
| Re=450 | Data | Hybrid | Cubic Upwind | Van Albada |
| $X_1/H$ | 9.5 | 8.79 | 9.13 | 9.06 |
| $X_2/H$ | 7.6 | 7.66 | 8.26 | 8.09 |
| $X_3/H$ | 11.3 | 11.14 | 11.39 | 11.52 |
| $dX/H$ | 3.7 | 3.48 | 3.13 | 3.43 |

Although no grid-refinement studies have been performed, the results are in fairly good agreement with the data. In fact, the results are better than those reported by Freitas(1995) for other general-purpose codes. The measurements indicate that for Re>450, 3d effects become significant, and for Re >6,600 the flow is 2d and fully turbulent.

**N104: 2D Scalar Convection with Recirculation:** The problem considered is pure 2d convection of scalar step in a prescribed recirculating velocity field. The flow geometry is a rectangular domain of 2 units length (x) and unit height (y). The flow enters through the inlet in the range x=(-1,0), and then circulates clockwise through 180 degrees to exit in the range x=(0,1). At the inlet, the scalar C=0 for x in the range (-1,-0.5) and C=1 in the range (0,1). Since physical diffusion is absent, this step change should be convected by the recirculating flow so as to appear as a step change at the outlet; thus, the exact solution is C=1 for x in the range (0,0.5) and C=0 for x in the range (0.5,1). The example compares the solution for 6 different linear schemes and 9 non-linear schemes.

This test case was devised by Smith and Hutton (1982) so as to provide a searching test of numerical convection schemes, especially for schemes based on 1d considerations. The velocity field is prescribed as shown in Figure 10.4 and is given by: $U = 2*y*(1-x^2)$ and $V = -2*x*(1-y^2)$ with x in the range (-1,+1) and y in the range (0,1).

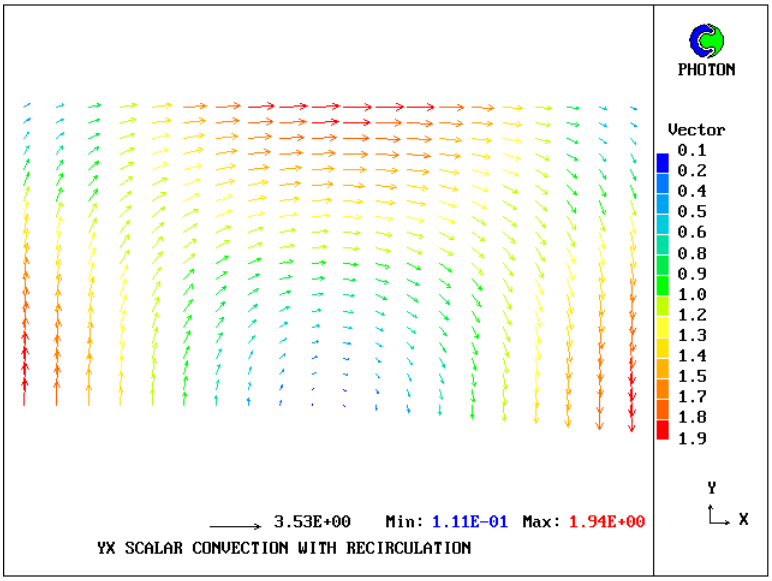


**Figure 10.4: Recirculating Scalar Convection: Velocity Field**

Figures 10.5 and 10.6 compare predictions on a 20 by 20 mesh for selected schemes with the exact solution for the outlet concentration profile. Figure 10.5 presents results for linear schemes, whereas Figure 10.6 shows results obtained with non-linear schemes. The UDS is too diffusive and all the linear higher-order schemes produce non-physical over- and undershoots. The Superbee schemes fares best of the selected non-linear schemes and produces reasonable agreement with the exact solution.

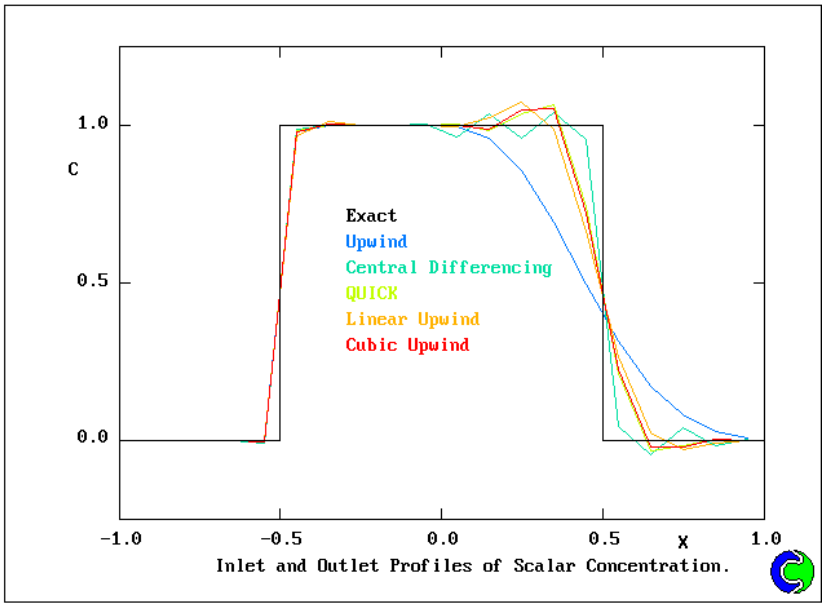


**Figure 10.5: Recirculating Scalar Convection: Concentration Outlet Profiles using Linear Schemes**

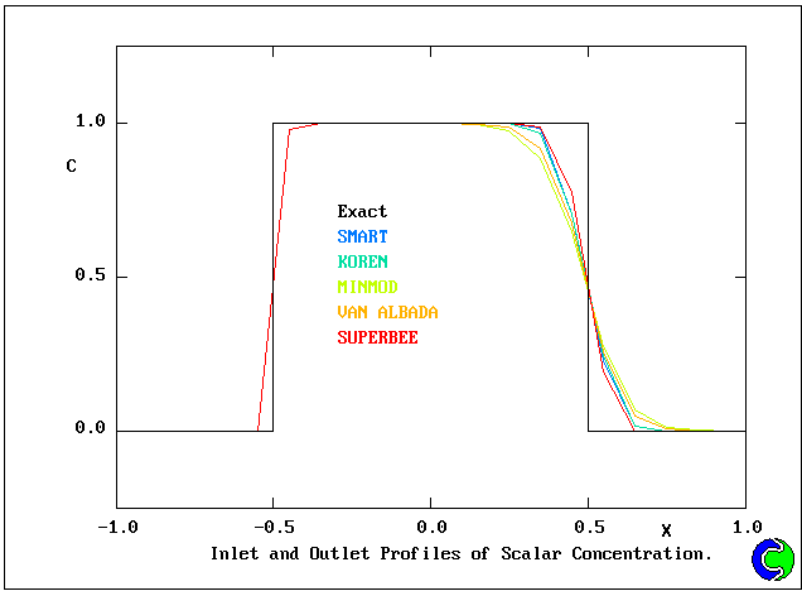


**Figure 10.6: Recirculating Scalar Convection: Concentration Outlet Profiles using Non-Linear Schemes**

Figure 10.7 compares the contours of scalar concentration produced by the UDS and Superbee schemes. This figure clearly shows the superiority of the Superbee scheme.

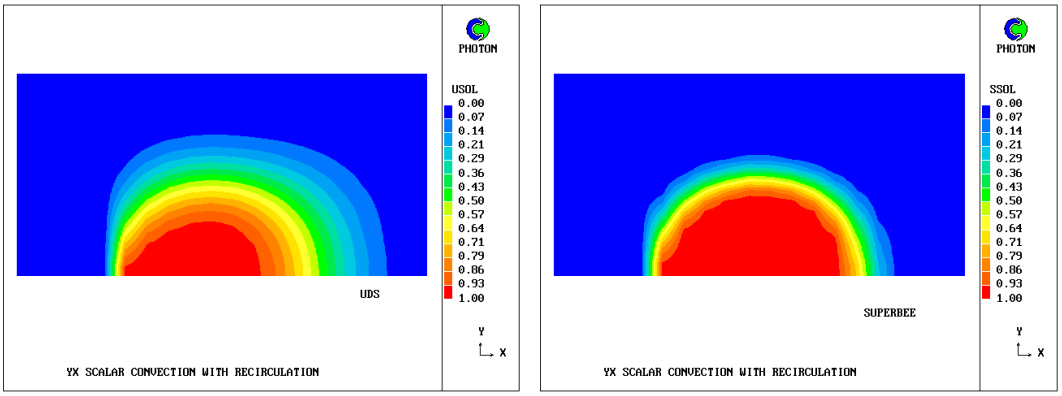


**Figure 10.7: Recirculating Scalar Convection: Concentration Contours for the UDS and Superbee Scheme.**

**N105: 2D Turbulent Backward-Facing Step:** The problem considered is 2d steady turbulent flow over a backward facing step, as studied experimentally Moss et al (1977). The Reynolds number based on step height H is $5.10^4$ and the expansion ratio is 1.1. The inlet is specified as a uniform inflow located 12H upstream of the step. The outlet plane is located 30H downstream of the step. The simulation uses QUICK for the velocities, and Koren's bounded scheme for the turbulence variables.

The configuration is similar to that of Kim et al (1980), as studied numerically throughout the PHOENICS Library (see e.g. library cases T103 &T305) and by many

others (see for example Thangam & Speziale (1992)). The present geometry has a smaller expansion ratio and slightly higher Reynolds number.

The measured reattachment length for this case is $X_r/H=5.5$, as measured from the step. The default computation using higher-order differencing schemes predicts a reattachment length of $X_r/H=4.74$. The PHOENICS default of HDS predicts $X_r/H=4.43$. A mesh of 30 vertical by 65 horizontal cells has been used in the calculations.

**N108: 2D Laminar Flow over a Fence:** The case considered is 2d laminar incompressible flow over a thin fence of height H located in a planar channel with a blockage ratio S/H=0.75. The flow Reynolds number is 82.5 based on fence height S and inlet bulk velocity $U_{in}$. This situation has been studied experimentally and numerically by Carvalho et al (1987). The inlet conditions employ a fully-developed parabolic velocity profile located 8 fence heights upstream of the fence, and an outlet condition of fixed pressure is applied 15 fence heights downstream of the fence. In practice the fence thickness is t/H=0.133, but in the calculations it is taken as zero.

The calculation is performed in all six planes as a consistency test, and computations are made with both the LUS and HDS for momentum. A mesh of 24 vertical by 48 horizontal cells has been used in the calculations.

Experiments indicate that a primary recirculation zone develops behind the fence with a reattachment length of $X_1/S=4.4$, as measured from the fence. An additional separation cell forms on the upper wall of the channel with the separation point located at $X_2/S=4.0$ and the reattachment point at $X_3/S=6.0$, yielding a separation length of dX/S=2.0. The main results are summarised in the table below:

| | Data | HDS | LUS |
|---|---|---|---|
| $X_1/s$ | 4.4 | 5.56 | 4.96 |
| $X_2/s$ | 4.0 | 4.21 | 3.85 |
| $X_3/s$ | 6.0 | 6.72 | 8.62 |
| dX/s | 2.0 | 2.51 | 4.77 |

Although no grid-refinement studies have been performed, the results are in reasonable agreement with the data.

**N110: 2D Turbulent Flow through an Orifice:** The case considered is 2d turbulent axisymmetric incompressible flow through an orifice plate of 11mm thickness located in a pipe. The pipe diameter D is 92mm and the hole in the orifice plate has a diameter H of 64 mm. The flow Reynolds number is 75,000 based on D and the inlet bulk velocity $U_{in}$. The orifice plate has practical value as a flowmeter.

The present case has been studied experimentally and numerically by Erdal (1997). The boundary conditions correspond to an inlet flow of fully-developed turbulent flow located 10D upstream of the plate, and an outlet condition of fixed pressure 17.5D downstream of the plate, and no-slip conditions at the walls. Turbulence is represented via the standard k-ε model plus wall functions, the LUS is used for momentum and the van-Leer harmonic scheme for k and ε.

The calculation employs 85 axial grid cells, of which 16 are located within the orifice plate, 31 upstream and 38 downsteam of the plate. The solution is known to be sensitive to the grid spacing in the vicinity of the upstream edge of the orifice plate, and grid independence is not accomplished with the current mesh. In particular, the recirculation zone within the orifice requires greater resolution in order to model accurately the radial extent of the vena contracta, and hence the pressure drop across the orifice plate. The measured pressure drop across the whole domain is 430 Pa, whereas the hybrid scheme predicts 322 Pa and the LUS yields 372 Pa.

**N111: 1D Shock-Free Transonic Nozzle Flow:** This case concerns steady 1d inviscid transonic flow through a Laval nozzle. The nozzle geometry is designed to produce a linear distribution of the Mach number M under shock-free conditions (see Malin [1977]). The flow is asymmetric about the throat with subsonic axial inflow and supersonic outflow. The dimensionless nozzle length is X=3 and the throat area is unity. The inlet conditions are prescribed total pressure $P_o$ and total temperature $T_o$ at M=0.5. The design outlet Mach number is 2.0, for which the exit pressure is 0.1278 $P_o$. This case serves mainly to verify the implementation of the schemes for compressible flow.

Computations are made with the UDS and the bounded higher-order UMIST scheme. So as to allow a direct computation of dimensionless flow variables, the flow equations are normalised such that the flow variables can be interpreted as: $P/P_o$; $\rho/\rho_o$; $T/T_o$; and $U^*\sqrt{(\gamma)}/a_o$. Here, $a_o$ is the acoustic velocity at $T_o$ (see Palacio et al [1990] ).

The results are not shown here, but both sets of results agree with the analytical solution. For shock-free flow the UMIST scheme offers no advantage over the UDS.

**N112: 1D Shocked Transonic Nozzle Flow:** This case is the same case as N111, but with a back pressure of 0.744Po, implying a normal shock at X=2.4. Compressibility corrections to the PHOENICS momentum equations are used so as to obtain acceptable shock predictions (see Malin & Sanchez [1988]). For this case PHOENICS without these corrections produces a shock at the exit plane because the in-line convection flux in the momentum equation uses an averaged density rather than the upwind density. If the upwind density were used, as in GXHOCS, the shock would be predicted somewhat down of its physical location. The compressibility corrections arrange that this flux is computed by averaging the continuity fluxes, thereby ensuring that the shock is predicted in the correct location.

The numerical and analytical data are compared in Figure 10.8 in terms of the axial distribution of static pressure. The results show that the higher-order UMIST scheme produces a much sharper shock than the UDS.

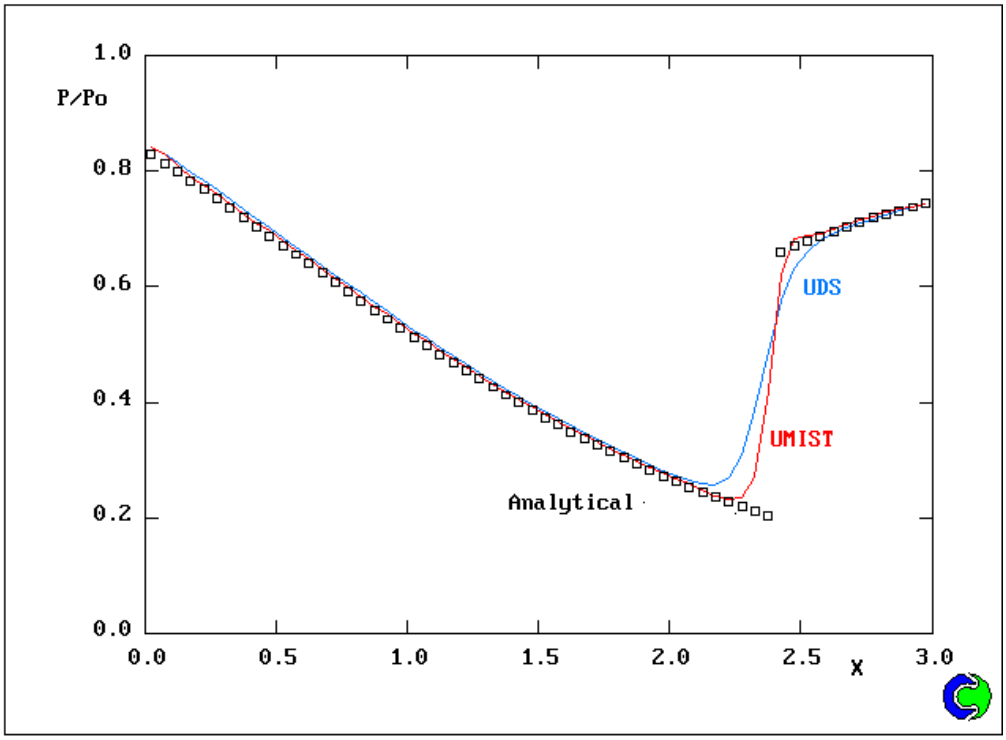


**Figure 10.8: Shocked Transonic Nozzle Flow: Static Pressure Distribution**

**N113: 2D Transonic Underexpanded Jet:** The problem considered is an axisymmetric sonic jet discharging into stagnant surroundings from a nozzle at a pressure 3.56 times higher than the ambient pressure. The stagnation enthalpy of the nozzle fluid is equal to that of the free stream, so that with the assumption of unit Prandtl numbers the energy equation need not be solved. The turbulence is represented by means of the k-ε turbulence model. Calculations are made with the HDS and the van-Leer MUSCL scheme. A relatively coarse mesh of 40 radial by 150 axial cells is used in the computations. This case was studied experimentally by Donaldson and Snedeker [1971] and numerically by Palacio et al [1990] .

The measurements and predictions are compared in Figure 10.9 in terms of the axial distribution of Mach number along the flow axis. The flow shows a rapid initial expansion of the nozzle fluid, with the experiments indicating Mach-disc formation at z/D=1.54 with a Mach number of 3.5 just upstream of the disc and a Mach number of 0.5 just downstream of the disc. Figure 10.9 shows that the MUSCL and HDS predictions reproduce the measurements fairly well, with the MUSCL scheme faring best and producing a sharper shock front. It is evident that a finer mesh is required to improve the accuracy of the predictions.

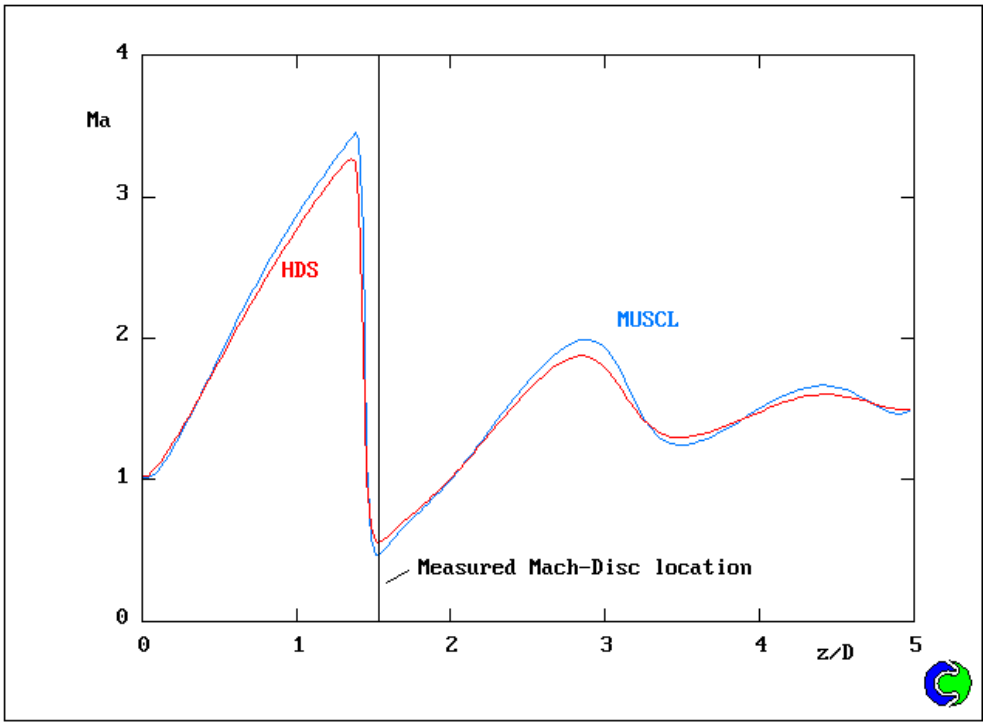


**Figure 10.9: Transonic Underexpanded Jet: Mach Number Distribution**

**N114: 2D Bluff-Body Stabilised Methane Jet:** The case considered is 2d steady, axisymmetric, turbulent non-reacting flow behind a bluff-body flame holder. The flow configuration consists of a 5.4mm diameter methane jet separated from an outer, annular air flow by a 50mm diameter bluff body. The flow is characterised by reverse flow in the annular air stream and exhibits well-defined fuel and annular air stagnation points along the centre-line. This case has been studied experimentally by Schefer et al (1987]) and was the subject of an ASCF Ercoftac CFD Workshop(see Garreton and Simonin (1994) ).

The measured fuel stagnation point is located 38.7mm downstream of the body while the air stagnation point occurs at about 63mm. The table below compares these experimental values with those computed using the HDS and the non-linear OSPRE scheme.

| | HDS Predictions | OSPRE Predictions | Measurements |
|---|---|---|---|
| Fuel $X_{stag}$ | 25.70 mm | 27.70 mm | 38.70 mm |
| Air $X_{stag}$ | 57.60 mm | 59.50 mm | 63.00 mm |

These results support the findings of other workers ( see for example McGuirk et al [1985] and Durao et al [1991] ), namely that: the problem requires very high

computational resolution for numerical accuracy; and like for other disk-related predictions, the standard k-ε model underestimates the size of the recirculation zone, and hence the location of the first stagnation point. The OPSRE scheme offers marginal improvement over the HDS.

The computation of the near field of these type of flows are known to be sensitive to the inlet conditions, and no assessment has been made in the present study on the influence of inlet values. In addition, no grid refinement studies have been carried out.

## 11.CONCLUSIONS

This paper has described development work conducted in 1995 to provide PHOENICS V2.2 and later releases with an extensive set of higher order schemes. The schemes comprised 5 linear and 12 non-linear schemes. Some successful applications of these schemes were described and placed in the PHOENICS Input Library and Applications Album.

More development needs to be done, including: extensions to include the volume-fraction variables R1, R2 and RS, and the energy variables TEM1 and TEM2; extensions to handle cells adjacent to external and internal boundaries; and the unification of these schemes with those currently provided for the co-located multi-block CCM and GCV options.

## 12.REFERENCES


1. R.K.Agrawal, 'A third-order accurate upwind scheme for Navier-Stokes at high Reynolds numbers', AIAA 81-0112, (1981).

2. B.F.Armaly, F.Durst, J.C.F.Pereira and B.Schonung, 'Experimental and theoretical investigation of backward-facing step flow', J.Fluid Mech., Vol.127, p473, (1983).

3. M.G.Carvalho, F.Durst and J.C.F.Pereira, 'Predictions and measurements of laminar flow over two-dimensional obstacles', Appl.Math.Modelling, Vol.11, p23, (1987).

4. R.Courant, E.Isaacson and M.Rees, 'On the solution of non-linear hyperbolic differential equations by finite differences', Comm. Pure Appl. Maths, 5, p243, (1952).

5. C.Donaldson and R.S.Snedeker, 'A study of free-jet impingement. Part 1. Mean Properties of free and impinging jets', J.Fluid Mech, 45, p281, [1971].

6. D.F.G.Durao, G.Knittel, J.C.F.Pereira and J.M.P.Rocha, 'Measurements and modelling of the turbulent near wake flow of a disk with a central jet, Proc. 8th Turbulent Shear Flows Conference, Technical University of Munich, 17.5, (1991).

7. A.Erdal, 'Computational analysis of the flow field downstream of flow conditioners', PhD Thesis, NUST, Trondheim, Norway, (1997).

8. C.J.Freitas, ‘Perspective: Selected benchmarks from commercial CFD codes’, ASME J.Fluids Engng, Vol.117, p208, (1995).

9. P.H.Gaskell and A.K.C.Lau, 'Curvature-compensated convective transport: SMART, a new boundedness-preserving transport algorithm, Int.J.Num.Meth.Fluids, Vol.8, p617, (1988).

10. D.K.Gartling, ‘A test problem for outflow boundary conditions- flow over a backward facing step’, Int.J.Num.Meth.Fluids, Vol.11, p953, (1990).

11. D.Garreton and O.Simonin, ‘Aerodynamics of steady state combustion chambers and furnaces’, ASCF Ercoftac CFD Workshop, October 17-18, Org: EDF, Chatou, France, (1994).

12. U.Ghia, K.N.Ghia and C.T.Shin, ‘High-Re solutions for incompressible flow using the Navier-Stokes equations and a multigrid method’, J.Comp.Physics, Vol.48, p387, (1982).

13. P.M.Gresho, D.K.Gartling, J.R.Torczynski, K.A.Cliffe, K.H.Winters, T.J.Garrett, A.Spence and J.W.Goodrich, ‘Is the steady viscous incompressible flow over a Backward-facing step at Re=800 stable?, Int.J.Num.Meth.Fluids Vol.17, p501 (1993).

14. A.Harten, 'On a class of high resolution total-variation stable finite-difference schemes', SIAM J.Num.Analysis, 21,p1, (1984).

15. J.E.Fromm, 'A method for reducing dispersion in convective difference schemes', J.Comp.Phys., Vol.3, p176, (1968).

16. C.Hirsch, 'Numerical computation of internal and external flows', Computational Methods for Inviscid and Viscous Flows, Vol.2,Wiley Interscience, (1990).

17. J.Kim, S.J.Kline and J.P.Johnston, ‘Investigation of a reattaching turbulent shear layer: Flow over a backward-facing step’, ASME J.Fluids Engng, Vol.102, p302, (1980).

18. B.Koren, 'A robust upwind discretisation method for advection, diffusion and source terms', In: Numerical Methods for Advection-Diffusion Problems, Ed. C.B.Vreugdenhil & B.Koren, Vieweg, Braunschweig, p117, (1993).

19. P.K.Khosla and S.G.Rubin, 'A diagonally dominant second-order accurate implicit scheme', Computers & Fluids, Vol.2, p207, (1974).

20. B.P.Leonard, M.A.Leschziner and J.McGuirk, 'The QUICK algorithm: a uniformly 3rd-order finite-difference method for highly convective flows', Proc. 1st Conf. on Numerical Methods in Laminar & Turbulent Flow, Swansea, p807, (1978).

21. B.P.Leonard, 'A stable and accurate convective modelling procedure based on quadratic upstream interpolation', Comp. Meth. Appl. Mech. Eng., Vo.19, p59, (1979).

22. B.P.Leonard, 'Locally-modified QUICK scheme for highly convective 2D and 3D flows', Proc. 5th Conf. Num. Meth. in Laminar and Turbulent Flow, Montreal, p35, (1987).

23. B.P.Leonard, 'Simple high-accuracy resolution program for convective modelling of discontinuities', Int.J.Num.Meth. Fluids, Vol.8, p1291, (1988).

24. F.S.Lien and M.A.Leschziner, 'Upstream monotonic interpolation for scalar transport with application to complex turbulent flows', Int.J.Num.Meth.Fluids, Vol.19, p527, (1994).

25. M.R.Malin, 'Calculation of two-dimensional flow in axial turbomachinery cascades', MSc Thesis, University of London, (1977).

26. M.R.Malin and L.Sanchez, 'One-dimensional steady transonic shocked flow in a nozzle', PHOENICS J., Vol.1, No.2, p214, (1988).

27. J.J.McGuirk, C.Papadimitriou and A.M.K.P.Taylor, 'Reynolds stress model calculations of two-dimensional plane and axisymmetric recirculating flows', Proc. 5th Turbulent Shear Flows Conference, Cornell Univ., USA, (1985).

28. W.D.Moss, S.Baker and L.J.S.Bradbury, 'Measurements of mean velocity and Reynolds stresses in some regions of recirculating flow', 1st Symp. on Turb. Shear Flows, Univ. Park, Penn., USA, Vol.II, p13.1, (1977).

29. B.Noll, 'Evaluation of a bounded high-resolution scheme for combustor flow computations', AIAA J., Vol.30, No.1, p64, (1992).

30. A.Palacio, M.R.Malin, N.Proumen and L.Sanchez, 'Numerical computations of steady transonic and supersonic flow fields', Int.J.Heat Mass Transfer, Vol.33, No.6, p1193, [1990]

31. H.S.Price, R.S.Varga and J.E.Warren, 'Applications of oscillation matrices to diffusion-convection equations', J.Math. & Phys., Vol.45, p301, (1966).

32. P.L.Roe, 'Finite-volume methods for the compressible Navier-Stokes equations', Proc. 5th Int. Conf. Num. Methods in Laminar and Turbulent Flow, Montreal, Vol. V, p2088, (1987).

33. P.L.Roe, 'Characteristic-based schemes for the Euler equations', Ann.Rev.Fluid Mech., 18, p337, (1986).

34. P.L.Roe, 'A survey of upwind differencing techniques', CFD Lecture Series 1989-04, VKI, Rhode-Saint-Genese, Belgium, (1989).

35. S.G.Rubin and P.K.Khosla, 'Polynomial interpolation method for viscous flow calculations', J.Comp.Phys., Vol.27, p153, (1982).

36. R.W.Schefer, M.Namazian and J.Kelly, 'Velocity measurements in a turbulent non-premixed bluff-body stabilised flame', Comb.Sci.&Tech., Vol.56, p101, (1987).

37. R.M.Smith and A.G.Hutton, 'The numerical treatment of advection: A performance comparison of current methods', Num.Heat Transfer, Vol.5, p439, (1982).

38. D.B.Spalding, 'A novel finite-difference formulation for differential expressions involving both first and second derivatives', Int.J.Num.Meth.Eng., Vol.4, p551, (1972).

39. S.P.Spekreijse, 'Multigrid solution of the steady Euler equations', PhD Thesis, TUD, Delft, The Netherlands, (1986).

40. P.K.Sweby, 'High resolution schemes using flux-limiters for hyperbolic conservation laws', SIAM J.Num.Anal., 21, p995, (1984).

41. S.Thangam and C.G.Speziale, 'Turbulent flow past a backward-facing step: A critical evaluation of two-equation models', AIAA J, Vol.30, No.5, p1314, (1992).

42. G.D.Van Albada, B.Van Leer and W.W.Roberts, 'A comparative study of computational methods in cosmic gas dynamics', Astron. Astrophysics, Vol.108, p76, (1982).

43. B.Van Leer, 'Towards the ultimate conservative difference scheme II', J.Comp.Phys., Vol.14, p361, (1974).

44. B.Van Leer, 'Towards the ultimate conservative difference scheme V', J.Comp.Phys., Vol.32, p101, (1979).

45. B.Van Leer, 'Upwind difference methods for aerodynamic problems governed by the Euler equations', Lectures in Applied Maths, 22, p327, Am.Math.Soc., (1985).

46. N.P.Waterson and H.Deconinck, 'A unified approach to the design and application of bounded higher-order convection schemes', VKI Preprint 1995-21, (1995).

47. N.P.Waterson, 'Development of bounded higher-order convection scheme for general industrial applications', VKI Project Report 1994-33, (1994).

48. G.Zhou, 'Numerical simulations of physical discontinuities in single and multi-fluid flows for arbitrary Mach numbers', PhD Thesis, Chalmers Univ. of Tech., Goteborg, Sweden (1995).

49. J.Zhu and W.Rodi, 'A low dispersion and bounded convection scheme', Comp.Meth. Appl. Mech. & Engng, Vol.92, p225, (1991).

50. J.Zhu, 'On the higher-order bounded discretisation schemes for finite-volume computations of incompressible flows', Comp.Meth.Appl.Mech. & Engng., Vol.98, p345, (1992).